Materials Letters 108 (2013) 311–315

Contents lists available at SciVerse ScienceDirect

Materials Letters

journal homepage: www.elsevier.com/locate/matlet

# Electrochemical performance of heteroatom-enriched amorphous carbon with hierarchical porous structure as anode for lithium-ion batteries

Young Soo Yun, Hyoung-Joon Jin *

*Department of Polymer Science and Engineering, Inha University, Incheon 402-751, Korea*

ARTICLE INFO

*Article history:*
Received 17 May 2013
Accepted 6 July 2013
Available online 15 July 2013

*Keywords:*
Heteroatom
Amorphous carbon
Hierarchical structure
Anode
Lithium-ion battery

ABSTRACT

Heteroatom-enriched amorphous carbon with hierarchical porous structure (HAC-HPS) was prepared for use as anode material for Li-ion batteries. The prepared HAC-HPS had open macroporous structure with a large number of nanopores and exhibited a high specific surface area of 1265.9 $m^2$/g. In addition, the prepared HAC-HPS had numerous heteroatoms, with 9.8 at% oxygen, 7.3 at% nitrogen, and 7.6 at% sulfur. The HAC-HPS showed superior electrochemical performance, including a high reversible capacity of 935 mAh/g, good rate performance, and great cycle stability over 275 cycles. The specific capacity increased continuously and reached 1090 mAh/g by the 270th cycle.



## 1. Introduction

Li-ion batteries (LIBs) are currently being used as one of the most important energy-storage devices for portable electronics and electrical/hybrid vehicles. However, the conventional graphite-based anode materials used in commercial LIBs have low Li-storage capacity (372 mAh/g) because of the limited Li-ion-storage sites ($LiC_6$) within the $sp^2$ carbon hexahedrons and relatively low rate capability, which results from the poor intercalation kinetics in the layered graphitic structures [1,2]. Recently, amorphous carbon has been considered as an alternative anode material for LIBs because of their relatively high Li-storage capacity [3,4].

The electrochemical behaviors of amorphous carbon differ from those of graphite in the following respects: (i) the redox-active potential range of amorphous carbon (1.2–0.0 V) is wider than that of the graphite electrode (0.5–0 V) [3]; (ii) the potential profile of amorphous carbon exhibits curve slopes without distinguishable plateaus, indicating electrochemically and geometrically nonequivalent Li ion sites, whereas the potential profile of graphite has the equivalent sites for a particular intercalation stage [5]; (iii) amorphous carbon exhibits large hysteresis between the charge and discharge potential profiles, which could be attributed to the ionic Li stored on the condensed aromatic ring in the unorganized carbon sites [6]; and (iv) amorphous carbon exhibits large irreversible capacity because of the formation of solid electrolyte interphase (SEI) films, which limits its usage as an anode material [7]. These differences in the electrochemical behavior of amorphous carbon compared to that of graphite are primarily induced by its disordered structure and heteroatoms [3–8]. Consequently, various studies analyzing the effects of the carbon structure and heteroatoms on the performance of amorphous carbon as an anode material for LIBs have been conducted. It has been reported that nitrogen or sulfur doping remarkably enhances the reversible capacity, rate capability, and cycle stability of amorphous carbon [9–13].

In addition, the porosity of carbon materials has also been demonstrated to be effective in enhancing the performance of amorphous carbon in LIBs [14–17]. For example, Zhang et al. have reported that the use of hierarchical porous carbon resulted in high rate performance by providing pathways for easy accessibility of the electrolytes and fast transportation of the Li ions [14]. Similarly, Qie et al. have reported that the presence of a large number of nanopores in the carbon materials can act as reservoirs for the storage of $Li^+$ ions. Furthermore, the large surface area provided by the porous structure facilitates sufficient electrode/electrolyte interface to absorb $Li^+$ ions and promotes rapid charge-transfer reactions [15]. These results imply that an ideal carbon-based anode material would be amorphous, contain numerous heteroatoms, and possess a hierarchical porous structure with a large number of nanopores.

Accordingly, in this study, we have prepared nitrogen-enriched amorphous carbon with hierarchical porous structure (NAC-HPS). Sulfur was additionally introduced to the NAC-HPS by thermal

* Corresponding author. Tel.: +82 32 860 7483; fax: +82 32 865 5178.
*E-mail address:* hjjin@inha.ac.kr (H.-J. Jin).

0167-577X/$ - see front matter © 2013 Elsevier B.V. All rights reserved.
http://dx.doi.org/10.1016/j.matlet.2013.07.026

treatment using elemental sulfur. The prepared heteroatom-enriched amorphous carbon with hierarchically porous structure (HAC-HPS) exhibited high capacity, good rate capability, and cycling stability as an anode material for LIBs.

## 2. Experimental

*NAC-HPS fabrication*: NAC-HPS was prepared using a previously reported procedure [18,19]. In the typical process, the reaction solution containing 7 wt% NaOH, 12 wt% urea, and 81 wt% water was prepared and precooled to −12 °C for 2 h. Next, 4 wt% cotton cellulose (Aldrich) was immersed in the solution, which was then intensely stirred for approximately 5 min at an ambient temperature to form an IC solution. The IC solution was then frozen at −196 °C and freeze-dried for 3 days. The resulting IC cryogel was carbonized from room temperature to 700 °C for 2 h at a heating rate of 10 °C/min with an Ar flow of 200 mL/min. After carbonization, the carbonized cryogel was washed using distilled water and ethanol and vacuum-dried at 30 °C for 24 h.

*HAC-HPS synthesis*: Following the preparation of NAC-HPS, the heteroatom was introduced by the following procedure. First, 100 mg of the prepared NAC-HPS was mixed with 100 mg of the elemental sulfur powder (Sigma-Aldrich, 99.98%) in a mortar. The mixture was thermally treated in a tubular furnace by ramping from room temperature to 600 °C or 1000 °C at a heating rate of 10 °C/min under an Ar flow rate of 200 mL/min. The reaction mixture was held at this temperature (600 °C or 1000 °C) for 2 h. The resultant product was stored in a vacuum oven at 30 °C without any washing process. For convenience, the samples obtained by annealing at 600 °C and 1000 °C are designated as HAC-HPS and HAC-HPS1000, respectively.

*Characterization*: The morphology of the prepared samples was observed using field emission transmission electron microscopy (FE-TEM; JEM2100F, JEOL, Japan). The porosity and specific surface area of the samples were analyzed from the nitrogen adsorption and desorption isotherms obtained at −196 °C by using the surface area and a porosimetry analyzer (ASAP 2020, Micromeritics, USA). In addition, X-ray photoelectron spectroscopy (XPS; PHI 5700 ESCA, Korea) was performed using the monochromated Al Kα radiation ($h\nu = 1486.6$ eV). The electrochemical performance of HAC-HPS and HAC-HPS1000 were evaluated using a Wonatech automatic battery cycler and CR2016-type coin cells. The coin cells were assembled in a glove box filled with Ar, employing a composite electrode with metallic Li foil and 1 M $LiPF_6$ (Aldrich 99.99%) dissolved in a solution of ethylene carbonate/dimethyl carbonate/diethyl carbonate (1:2:1 v/v) as the electrolyte. The cells were galvanostatically cycled between 0.01 and 3.0 V vs. $Li/Li^+$ at various current densities.

## 3. Results and discussion

Fig. 1(a) and (b) shows the TEM images of the prepared HAC-HPS under different magnifications. As evidenced from the TEM image, the HAC-HPS exhibited a porous structure over a large area, with open macropores of diameter ~200 nm. Moreover, the high-resolution TEM image indicated that the HAC-HPS had a disordered carbon structure with a large number of micropores. Therefore, the porosity and specific surface area of the HAC-HPS were investigated using nitrogen adsorption and desorption isotherms, as shown in Fig. 1(c) and (d). The nitrogen adsorption and desorption isotherms exhibited mixed IUPAC type I and type IV hystereses. This suggests the presence of dual microporous and

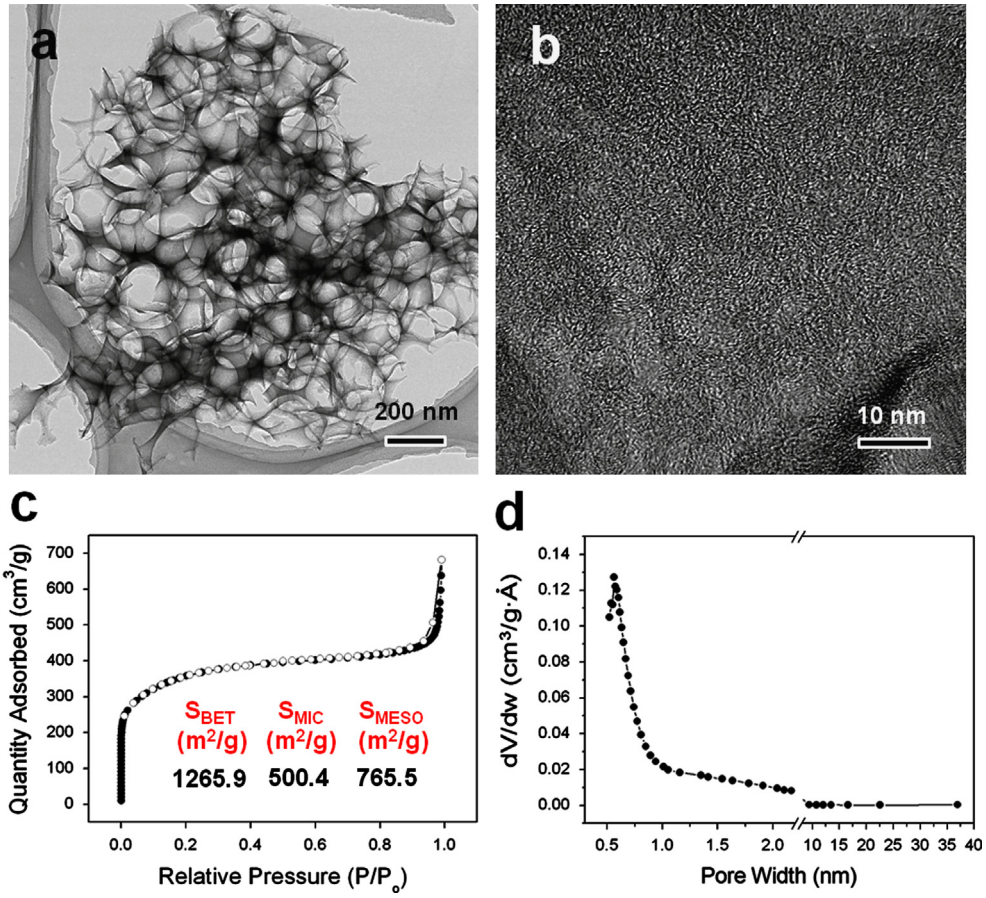


**Fig. 1.** (a,b) TEM images of HAC-HPS under different magnifications. (c) Nitrogen adsorption and desorption isotherm and (d) pore size distribution of HAC-HPS.

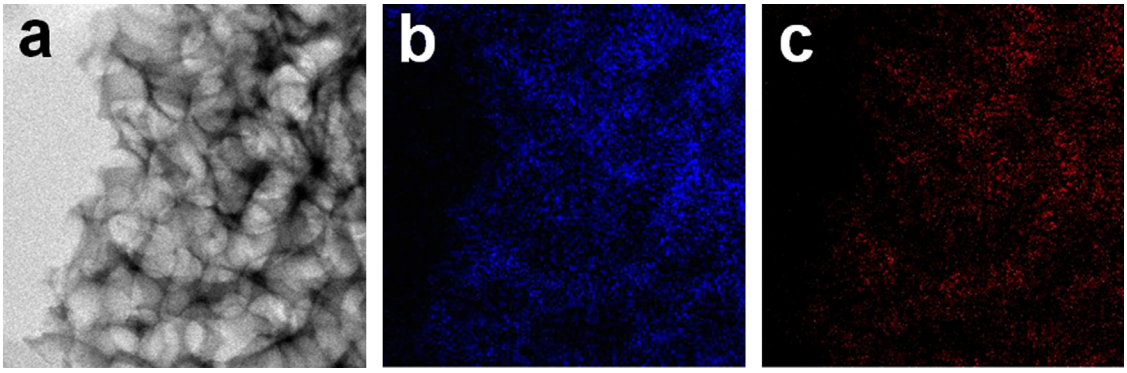


**Fig. 2.** EDX mapping data of HAC-HPS.

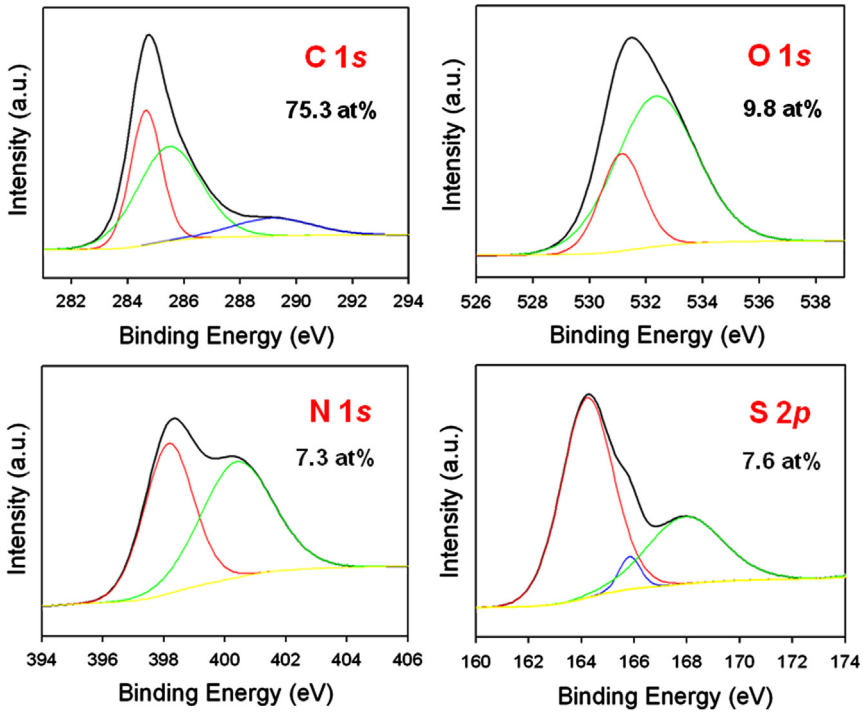


**Fig. 3.** XPS (a) C 1*s*, (b) O 1*s*, (c) N 1*s* and (d) S 2*p* spectra of HAC-HPS.

mesoporous structure (Fig. 1(c)). The specific surface area of the prepared HAC-HPS was determined to be 1265.9 $m^2/g$, which was composed of both micropores (500.4 $m^2/g$) and mesopores (765.5 $m^2/g$). Fig. 1(d) shows that pore size distribution in the sample. The surface of the HAC-HPS predominantly consisted of nanopores of size 5.6 Å.

The EDX mapping shows that sulfur atoms were homogeneously incorporated in all the surfaces of NAC-HPS (Fig. 2). The chemical configuration of the HAC-HPS was characterized by using XPS (Fig. 3). The XPS C 1*s* spectrum of the HAC-HPS revealed several distinct peaks, including the main C–C peak at 284.6 eV, C–O, C–N, and C–S centered at 285.5 eV, and C(O)O centered at 289.2 eV (Fig. 3(a)) [18–20]. On the other hand, the O 1s spectrum had two distinct peaks at 531.1 and 532.4 eV, corresponding to the oxygen atoms in the carbonyl groups and various other oxygen groups (Fig. 3(b)) [18–20]. Furthermore, the chemical configuration of the nitrogen atoms were found to be in the form of pyridinic N (398.2 eV) and pyrrolic N (400.4 eV).

Before thermal treatment with elemental sulfur, the oxygen and nitrogen contents of the NAC-HPS were determined to be 9.9 at% and 8.0 at%, respectively. After thermal treatment with elemental sulfur, the resulting sample (HAC-HPS) exhibited oxygen and nitrogen contents of 9.8 at% and 7.3 at%, respectively, which were very close to those obtained before thermal treatment (NAC-HPS), although 7.6 at% sulfur was doped into HAC-HPS after thermal treatment at 600 °C with elemental sulfur. Intriguingly, no new peaks were seen in the XPS C 1*s*, O 1*s*, and N 1*s* spectra of HAC-HPS, compared to that of NAC-HPS, except for the increase in the peak intensity of C–O bonds after thermal treatment at 600 °C with elemental sulfur. This could be attributed to the formation of C–$SO_x$ bond between oxygen and sulfur. This was experimentally verified by a peak at 167.9 eV corresponding to C–$SO_x$ bond in the XPS S 2*p* spectrum of the HAC-HPS. Additionally, two other peaks at 164.2 and 165.8 eV corresponding to the C–S and C=S bonds, respectively, could be observed [10,13,21]. Furthermore, to investigate the effects of heteroatoms, NAC-HPS was thermally treated with elemental sulfur at a higher temperature (1000 °C, HAC-HPS1000) than that used to obtain the HAC-HPS. The XPS spectra of HAC-HPS1000 indicated smaller amounts of oxygen, nitrogen, and sulfur (6.4, 3.2, and 2.5 at%, respectively) compared to those of the HAC-HPS.

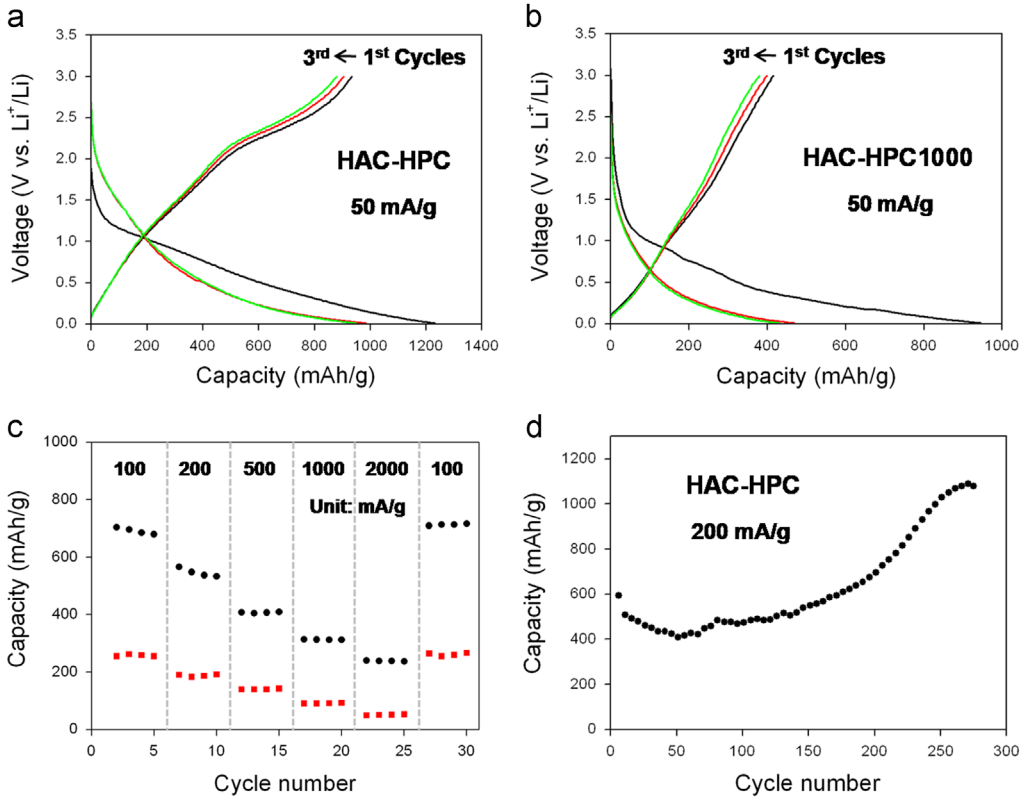


**Fig. 4.** Galvanostatic charge/discharge profiles of (a) HAC-HPS and (b) HAC-HPS1000 in potential range 0.01–3.0 V *vs.* $Li/Li^+$ at current density 50 mA/g. (c) Rate capability of HAC-HPS (black, circle) and HAC-HPS1000 (red, square) at various current densities from 100 to 2000 mA/g. (d) Cycling performance of HAC-HPS for 275 cycles at current density 200 mA/g. (For interpretation of the references to color in this figure legend, the reader is referred to the web version of this article.)

The electrochemical performance of both HAC-HPS and HAC-HPS1000 were evaluated via constant current charge/discharge cycling in the potential range 0.01–3.0 V at various current densities. The charge/discharge curves of the HAC-HPS and HAC-HPS1000 (Fig. 4(a) and (b), respectively) displayed similar profiles with relatively large voltage hysteresis, without any distinct potential plateaus, indicating the electrochemically and geometrically nonequivalent Li-ion sites. These are typical charge/discharge curves of disordered carbons. However, the redox-active potential range of HAC-HPS was found to be wider than that of HAC-HPS1000. In addition, hysteresis between the charge and discharge potential profiles of HAC-HPS was also higher than that of HAC-HPS1000. These results suggest the occurrence of more surface reactions in the case of HAC-HPS compared to that in HAC-HPS1000.

The first discharge and charge profiles of the HAC-HPS showed large specific capacities of approximately 1230 and 935 mAh/g, respectively, at a current density of 50 mA/g (Fig. 4(a)). The reversible capacity of HAC-HPS, which corresponds to that of $Li_{2.5}C_6$, was found to be more than twice the value of HAC-HPS1000 (415 mAh/g). The observed high reversible capacity could have been induced because of the increased number of active sites with heteroatoms. Further, the irreversible capacity of HAC-HPS remarkably reduced compared to that of HAC-HPS1000. This difference of the irreversible capacity could be induced because of several reasons, the most probable one being the effect of heteroatoms, because the two samples essentially differed only in their contents of heteroatoms. However, more specific investigations are required to understand the relationship between the irreversible capacity and the number of heteroatoms.

Fig. 4(c) shows the rate performance of HAC-HPS and HAC-HPS1000 from 100 to 2000 mA/g. In the case of HAC-HPS, stable capacities of ca. 240 mAh/g could still be obtained at a current density of 2000 mA/g, which was approximately four times higher than that for HAC-HPS1000. In addition, when the current density was reduced to 100 mA/g after 25 cycles, the initial reversible capacity of HAC-HPS was recovered, demonstrating very good reversibility. Fig. 4(d) shows the cycling stability of HAC-HPS for 275 charge/discharge cycles at a current density of 200 mA/g. The cycling stability was maintained for over 275 cycles, and the specific capacity increased continuously with cycling. The specific capacity started at 510 mAh/g and reached 1090 mAh/g by the 270th cycle. This result is similar to that of a previous report on N-doped multiwall carbon nanotubes [22]. This capacity increase could be rationalized by the fact that the number of active sites for Li-ion storage was increased during cycling because of the diffusion of the Li-ions into the internal nanopores [23,24].

## 4. Conclusion

HAC-HPS was prepared by thermal treatment of the as-prepared NAC-HPS at 600 °C with elemental sulfur. The prepared HAC-HPS had hierarchical porous structure and exhibited a high specific surface area of 1265.9 $m^2/g$. In addition, the HAC-HPS had numerous heteroatoms, with 9.8 at% oxygen, 7.3 at% nitrogen, and 7.6 at% sulfur. The electrochemical performance of the HAC-HPS was found to be superior to that of the HAC-HPS1000 (obtained by thermal treatment of NAC-HPS at 1000 °C with elemental sulfur). The HAC-HPS showed a high reversible capacity of 935 mAh/g at a current density of 50 mA/g, as well as good rate performance and great cycle stability over 275 cycles.

## Acknowledgments

This work was supported by the National Research Foundation of Korea Grant funded by the Korean government (MEST) (NRF-2010-C1AAA001-0029018), and also supported by Basic Science Research Program through the National Research Foundation of Korea (NRF) funded by the Ministry of Education (2013008534).

## References

[1] Sawai K, Ohzuku T. J Electrochem Soc 2003;150:A674.
[2] Guo B, Wang X, Fulvio PF, Chi M, Mahurin SM, Sun X-G, et al. Adv Mater 2011;23:4661.
[3] Kaskhedikar NA, Maier J. Adv Mater 2009;21:2664.
[4] Dahn JR, Zheng T, Liu Y, Xue JS. Science 1995;270:590.
[5] Winter M, Besenhard JO, Spahr ME, Novák P. Adv Mater 1998;10:725.
[6] Takami N, Satoh A, Ohsaki T, Kanda M. Electrochim Acta 1997;42:2537.
[7] Mukai SR, Hasegawa T, Takagi M, Tamon H. Carbon 2004;42:837.
[8] Naoi K, Ogihara N, Igarashi Y, Kamakura A, Kusachi Y, Utsugi K. J Electrochem Soc 2005;152:A1047.
[9] Weydanz WJ, Way BM, Buuren TV, Dahn JR. J Electrochem Soc 1994;141:900.
[10] Wu YP, Fang S, Jiang Y, Holze R. J Power Sources 2002;108:245.
[11] Ito S, Murata T, Hasegawa M, Bito Y, Toyoguchi Y. J Power Sources 1997;68:245.
[12] Ma C, Shao X, Cao D. J Mater Chem 2012;22:8911.
[13] Yan Y, Yin Y-X, Xin S, Guo Y-G, Wan LJ. Chem Commun 2012;48:10663.
[14] Zhang F, Wang K-X, Li G-D, Chen J-S. Electrochem Commun 2009;11:130.
[15] Qie L, Chen W-M, Wang Z-H, Shao Q-G, Li X, Yuan L-X, et al. Adv Mater 2012;24:2047.
[16] Ji L, Zhang X. Nanotechnology 2009;20:155705.
[17] Lee B-S, Son S-B, Park K-M, Lee G, Oh KH, Lee S-H, et al. ACS Appl Mater Interfaces 2012;4:6702.
[18] Yun YS, Shim J, Tak Y, Jin H-J. RSC Adv 2012;2:4353.
[19] Yun YS, Kim D, Park HH, Tak Y, Jin H-J. Synth Met 2012;162:2337.
[20] Yun YS, Cho SY, Shim J, Kim BH, Chang S-J, Baek SJ, et al. Adv Mater 2013;25:1993.
[21] Valade L, Fraxedas J, Caro DD, Savy J-P, Malfant I, Faulmann C, et al. J Low Temp Phys 2006;142:141.
[22] Shin WH, Jeong HM, Kim BG, Kang JK, Choi JW. Nano Lett 2012;12:2283.
[23] Li X, Geng D, Zhang Y, Meng X, Li R, Sun X. Electrochem Commun 2011;13:822.
[24] Kim G-P, Park S, Nam I, Park J, Yi J. J Mater Chem A 2013;1:3872.